Soft Matter

PAPER

View Article Online
View Journal

Cite this: DOI: 10.1039/c9sm01666j

Nuclear size changes caused by local motion of cell boundaries unfold the nuclear lamina and dilate chromatin and intranuclear bodies†

Aditya Katiyar, ‡[a] V. J. Tocco,‡[b] Yuan Li,[b] Varun Aggarwal,[b] Andrew C. Tamashunas, [b] Richard B. Dickinson[b] and Tanmay P. Lele *[b]

Received 16th August 2019,
Accepted 23rd October 2019

DOI: 10.1039/c9sm01666j

rsc.li/soft-matter-journal

The mechanisms by which mammalian nuclear shape and size are established in cells, and become abnormal in disease states are not understood. Here, we tracked motile cells that underwent systematic changes in cell morphology as they moved from 1-D to 2-D micro-patterned adhesive domains. Motion of the cell boundaries during cell motility caused a dynamic and systematic change in nuclear volume. Short time scales (~1 h) distinguished the dilation of the nucleus from the familiar increase that occurs during the cell cycle. Nuclear volume was systematically different between cells cultured in 3-D, 2-D and 1-D environments. Dilation of the nuclear volume was accompanied by dilation of chromatin, a decrease in the number of folds in the nuclear lamina, and an increase in nucleolar volume. Treatment of 2-D cells with non-muscle myosin-II inhibitors decreased cell volume, and proportionately caused a decrease in nuclear volume. These data suggest that nuclear size changes during cell migration may potentially impact gene expression through the modulation of intranuclear structure.

Introduction

Nuclear mechanics and morphology are characteristic of cell phenotype and become significantly abnormal in human pathologies. Unlike the smooth, ellipsoidal shape of normal nuclei, cancer nuclei tend to have highly abnormal nuclear shapes with irregular contours consisting of lobes and invaginations[1,2] which have prognostic and diagnostic significance.[3] The mechanisms by which nuclear shape becomes abnormal in human pathologies are not fully understood[4,5] but are thought to be related to changes in cell and nuclear mechanics.[1]

In addition to nuclear shape, nuclear size, as measured by its volume, also becomes significantly altered in human pathologies like cancer (reviewed in ref. 6). These alterations to nuclear size are not primarily due to alterations to DNA;[7] rather a key determinant of nuclear size in cells is the cytoplasmic volume. For example, nuclear size or volume has been shown to correlate with cell size in yeast.[8,9] Similarly, nuclear volume scales with cytoplasmic volume in *Xenopus* egg extracts.[10] In *Xenopus*, nuclear size sensitivity to the amount of cytoplasm around it may be due to the availability of cytoplasmic factors such as importin α[11] and dynein-dependent transport of lipid membranes.[10] Consistent with these studies, osmotically induced changes to cell volume cause proportionate changes to nuclear volume.[12,13]

Changes to actomyosin tension can also alter nuclear volume.[14–16] Because actomyosin tension is dynamically modulated during cell migration,[17,18] here we examined the extent to which local and dynamic changes in cell shape cause changes in nuclear volume. There was a substantial increase in nuclear volume as cells crawled on fibronectin-coated patterns from 1-D lines to 2-D rectangles. Nuclear dilation was accompanied by a corresponding decrease in folds in the nuclear lamina and dilation of chromatin and intranuclear bodies. Myosin inhibition reduced cell volume and caused a proportionate decrease in nuclear volume. These results demonstrate that nuclear size and intranuclear structure is dynamically controlled during cell crawling.

Results

Dynamic changes in nuclear volume are driven by changes in cell shape during cell migration

Fibroblasts *in vivo* have markedly elongated nuclear shapes, as seen in stained cross-sections of tissue. Such elongated, physiologically relevant phenotype of fibroblasts can be reproduced by culture in 3-dimensional collagen gels. We observed instances in collagen gel culture in which a narrow, elongated fibroblast locally widened as it migrated (an example is in Fig. 1A and

[a] *Department of Mechanical and Aerospace Engineering, University of Florida, Gainesville, FL 32611, USA*
[b] *Department of Chemical Engineering, University of Florida, Gainesville, FL 32611, USA. E-mail: tlele@che.ufl.edu*

† Electronic supplementary information (ESI) available. See DOI: 10.1039/c9sm01666j
‡ These authors contributed equally.

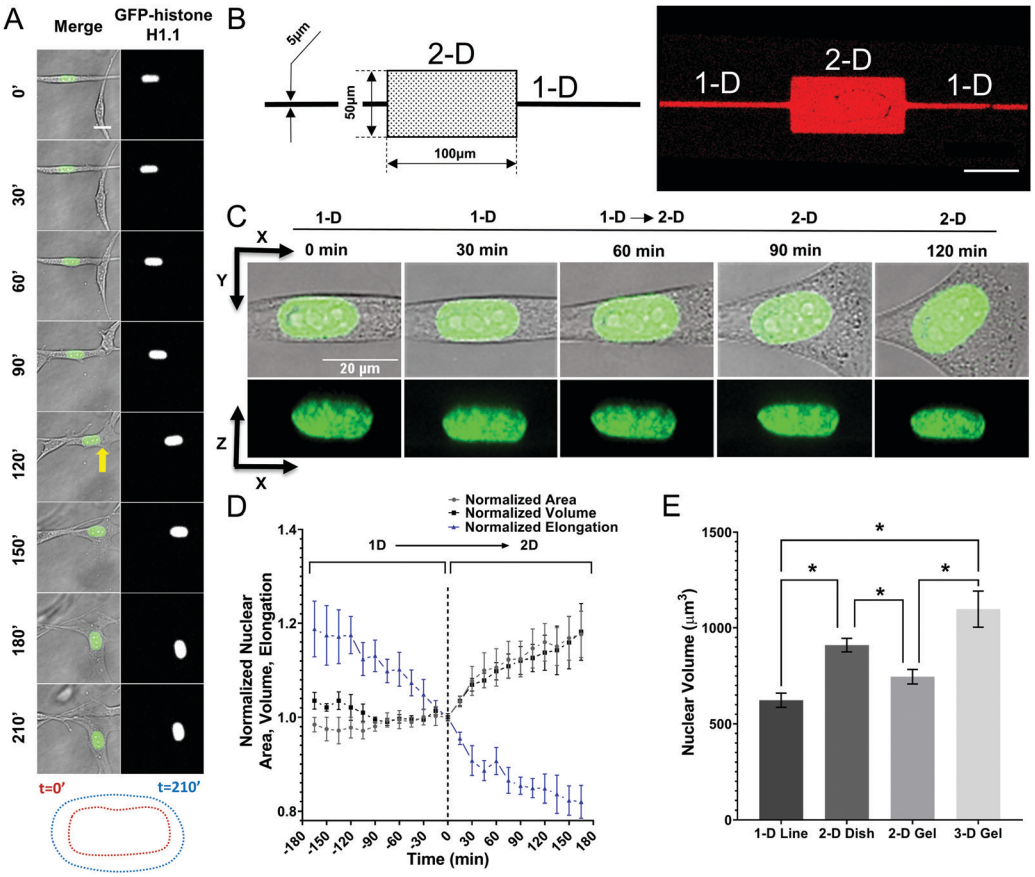

Fig. 1 Nuclear volume in migrating cells and in different culture conditions. (A) a migrating NIH3T3 fibroblast expressing GFP-histone H1.1 in 3-D collagen gel. The yellow arrow indicates local cell widening accompanied by nuclear widening. Scale bar is 20 μm. Dotted lines show a comparison between the nuclear boundary at time 0 and 210 minutes. (B) Left: Design of the pattern on a silicon master wafer used to make PDMS negative molds for micro-patterning. Right: An image of rhodamine-fibronectin micropatterned into 5 μm-wide 1-D lines that terminate into a 2-D rectangle. Scale bar is 50 μm. (C) Image shows x–y and x–z cross-sections of a GFP-histone H1.1 expressing nucleus as it migrates from the 1-D line to a 2-D rectangle. Scale bar is 20 μm. (D) Pooled plots of nuclear volume, nuclear x–y area, and nuclear x–y elongation (measured as width/length) over time during the transition from the 1-D to 2-D shapes. The time data for all cells was corrected such that $t = 0$ is the time at which the leading edge of the nucleus reached the edge to the 2-D fibronectin pattern. Data are mean ± SEM for 8 cells from at least 4 different experiments. (E) Nuclear volume of NIH 3T3 cells on 1-D fibronectin lines (36 cells), fibronectin-coated culture dishes (43 cells), upon collagen gels (34 cells), and cultured within collagen gels (36 cells). Data are mean ± SEM from three independent experiments. *$p < 0.05$ with Student's t-test.

Movie 1, ESI†). The shape of the GFP-histone H1.1 labeled nucleus coincided closely with the local shape of the cell; as the cell began to widen near the nucleus, the nucleus widened as well (yellow arrow in Fig. 1A). To study this shape-change more reproducibly, we micro-patterned the surface of a polymer coverslip with a fibronectin shape (Fig. 1B) consisting of a 5-micron-wide line (1-D) of sufficiently long length terminating in a 50-micron by 100-micron rectangle (2-D) (Fig. 1B). This pattern enabled the imaging of highly elongated fibroblasts on the narrow ("1-D") region as they approached and moved onto the broader ("2-D") region.

We performed laser-scanning confocal fluorescence microscopy of the GFP-histone labeled nucleus during migration from the 1-D to 2-D region, and examined the x–z and x–y views of the nucleus (Fig. 1C and Movie 2, 3, ESI†). Cell nuclei expanded in cross sectional area when they reached the interface between the 1-D and 2-D region, coinciding closely with the widened local cell shape (Fig. 1C, x–y view). As nuclei translated during migration from the 1-D to the 2-D region, the height decreased slightly (x–z plane images in Fig. 1C and Movie 3, ESI†) while the area of cross-section in the x–y plane widened significantly (x–y plane images in Fig. 1C). Such a significant increase in the area of cross-section was observed consistently across several cells over the ~450 min of migration from 1-D to the 2-D region (see pooled data in Fig. 1D). We quantified the nuclear volume from confocal z-stacks during the migration and observed a nearly 20% increase upon migration from the 1-D to the 2-D region (Fig. 1D, see also materials and methods for volume measurements and ref. 19). These results suggest that a widening of the cell shape during cell migration, which drives widening of the local nuclear shape, can increase the volume of the nucleus. The relatively short timescale of the volume changes (within 75 minutes) and the fact that they occur reproducibly upon migration from the 1-D to the 2-D pattern argues against the possibility that the nuclear volume changes are cell-cycle related. Also, these volume changes did not occur over a similar time frame when cells were on the 1-D line (Fig. 1D, −180 min to 0 min).

Fibroblasts on 1-D lines are more elongated than cells on 2-D areas, while fibroblasts in 3-D culture tend to have branched shapes. Given these differences in cell shape, we compared nuclear volumes between fibroblasts cultured overnight and then fixed on micropatterned fibronectin lines, on tissue culture dishes, inside three-dimensional collagen gels and on the surface of these gels. There were systematic differences in nuclear volume in these different culture conditions. Nuclear volumes on the 1-D lines and on the collagen gel surface were similar, and lower than the volume on 2-D tissue culture dishes, which was in turn lower than the volume in 3-D gels (Fig. 1E). These experiments reveal that there are systematic differences in fibroblast nuclear volume in different culture conditions.

Nuclear expansion dilates chromatin, unfolds the nuclear lamina and alters nuclear bodies

Chromatin is molecularly linked to the nuclear lamina,[20] which suggested to us that the observed increase in nuclear volume during migration could cause a dilation of chromatin. To test this hypothesis, we examined the fate of regions of chromatin in the nucleus as the nucleus dilated during cell migration from 1-D to 2-D fibronectin patterns. Chromatin regions were tracked by photoconverting Dendra2-histone H3.3, a protein stably integrated into nucleosomes,[21] in defined spatial regions, and then imaging its dynamics during nuclear shape changes. We first confirmed that the protein did not exchange and lose fluorescence in the photoactivated spot by tracking the fate of photoactivated Dendra2-histone H3.3 in fibroblasts. The photoactivated pattern was stable and did not blur over a time scale of two hours (Fig. S1, ESI†), which is longer than the time scale for nuclear widening (compare with Fig. 1C and D). Next, we tracked the change in the shape of a photoconverted spot as the nucleus migrated from the 1-D to the 2-D region. Because photoconversion is not confined to a single plane, we performed confocal imaging and captured multiple planes at different *z*-positions. Fig. 2A and Movie 4 (ESI†) shows a time lapse image sequence of a typical nucleus in which there is a clear expansion of the photoactivated spot upon nuclear expansion. Further, the

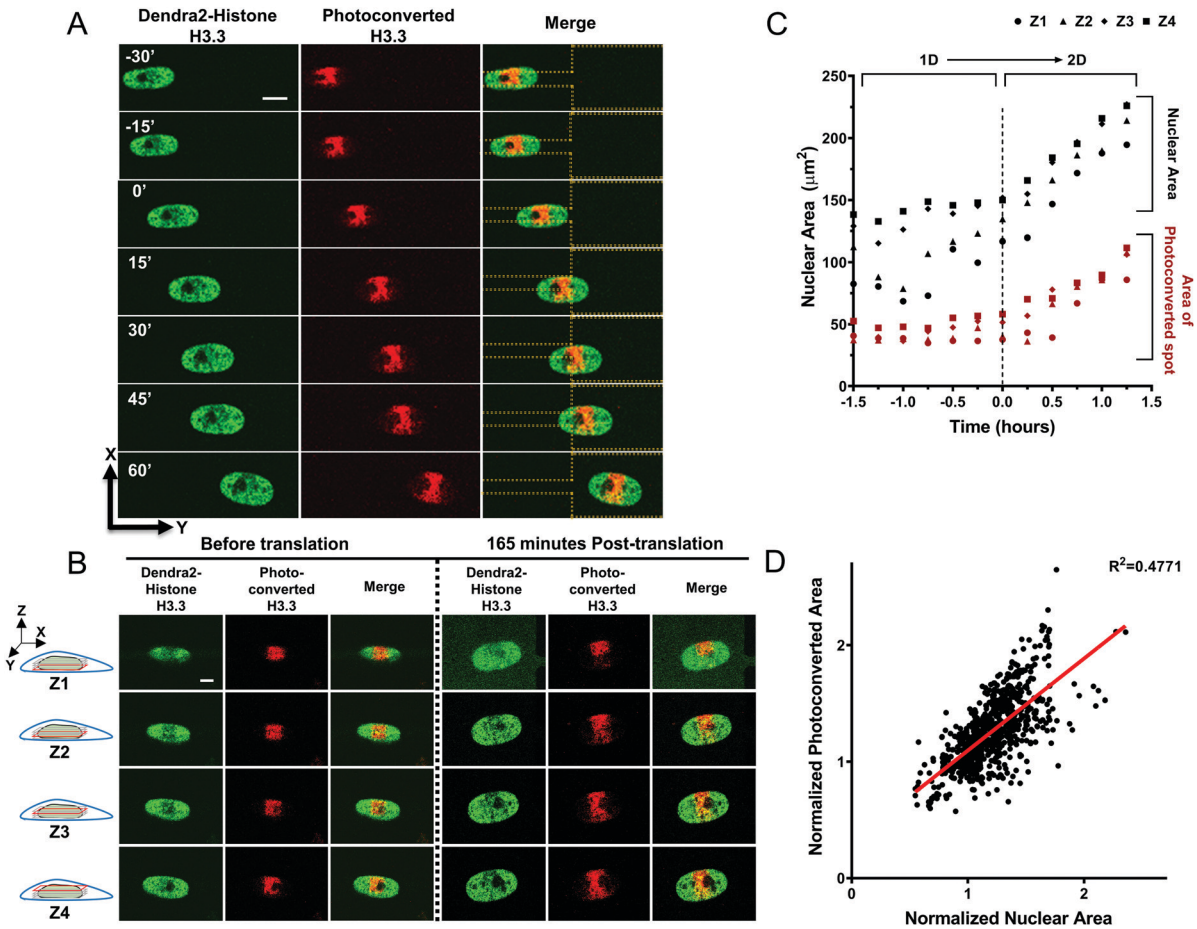

Fig. 2 Chromatin dilation during 1-D to 2-D migration. (A) Images show photoconverted Dendra2-histone H3.3 spot in an elongated nucleus in a cell on the 1-D fibronectin line, and the same nucleus tracked over time during and after translation onto the 2-D fibronectin area. Scale bar is 10 μm. (B) Images of the photoconverted spot in distinct confocal planes imaged at different vertical (*z*-axis) positions. Scale bar is 5 μm. (C) Quantification of nuclear area and area of photoconverted spot in the different image planes in (B) over time. (D) Scatter plot of normalized photoconverted area *versus* normalized nuclear area; data was pooled from time-lapse images of 8 different Dendra2-histone H3.3 expressing cells that migrated from 1-D to 2-D patterns. The red line was determined by linear regression; R^2 = 0.4771.

photoconverted spot in each confocal plane underwent a similar expansion (Fig. 2B and C). We pooled measured areas in different imaging planes and at different times from multiple cells migrating from 1-D to 2-D patterns, and found a strong correlation between normalized spot area and normalized nuclear area (Fig. 2D). These data collectively show that nuclear widening during cell migration causes chromatin expansion.

We asked if changes in nuclear volume in 1-D and 2-D cells altered the geometry of chromatin associated structures in the nucleus. Consistent with expansion of chromatin, Srm160 labeled splicing speckles which reside in interchromatin spaces[22] underwent a dynamic translation away from each other during the nuclear expansion (Fig. 3A). However quantitative comparisons of speckle geometry and volume between 1-D and 2-D nuclear shapes proved to be unreliable owing to their small size, and also network-like appearance in the nucleus. We therefore chose to quantify the volume of nucleoli stained for fibrillarin, which had a more condensed and discrete appearance in the fibroblast nucleus (Fig. 3B). Total nucleolar volume per cell was larger in 2-D culture than in 1-D culture consistent with the corresponding nuclear volume differences. These results show that nuclear volume dilation caused by local widening of the cell body cause a dynamic dilation of intranuclear structures like chromatin, nucleoli and intranuclear bodies like splicing speckles, all of which may potentially alter key cellular processes like gene expression.

We have previously proposed that the flattening of the nucleus during cell spreading reaches a steady state when the wrinkled nuclear lamina in the rounded nucleus becomes fully unfolded during the process of flattening. As the nucleus similarly reached a steady state shape after migrating from the 1-D to the 2-D pattern, we examined the spatial distribution of GFP lamin A in fibroblasts during the migration. Fig. 3C and Movie 5 (ESI†) shows a single nucleus migrating from the 1-D pattern to the 2-D pattern. On the 1-D pattern, folds were observed in the GFP lamin A expressing nucleus throughout the time it was on the 1-D line. These folds gradually disappeared as the nucleus widened during the transition from the 1-D to 2-D pattern (Fig. 3C left panel). The texture in the GFP lamin A images (corresponding to folds, wrinkles, holes *etc.*) disappeared from each of the confocal planes imaged during the transition (Fig. S2, ESI†) while, in the reverse transition of the cell from a 2-D area onto 1-D line, the folds reappeared (Fig. 3C (right) and Movie 6, ESI†). Also, immunostaining of lamin A/C revealed consistent folds/wrinkles in the nucleus on 1-D lines, while these folds were largely absent on 2-D areas (Fig. 3D). We quantified texture in the nuclear cross-section as the number of pixels in grooves, folds, holes, and wrinkles (excluding the nuclear periphery;

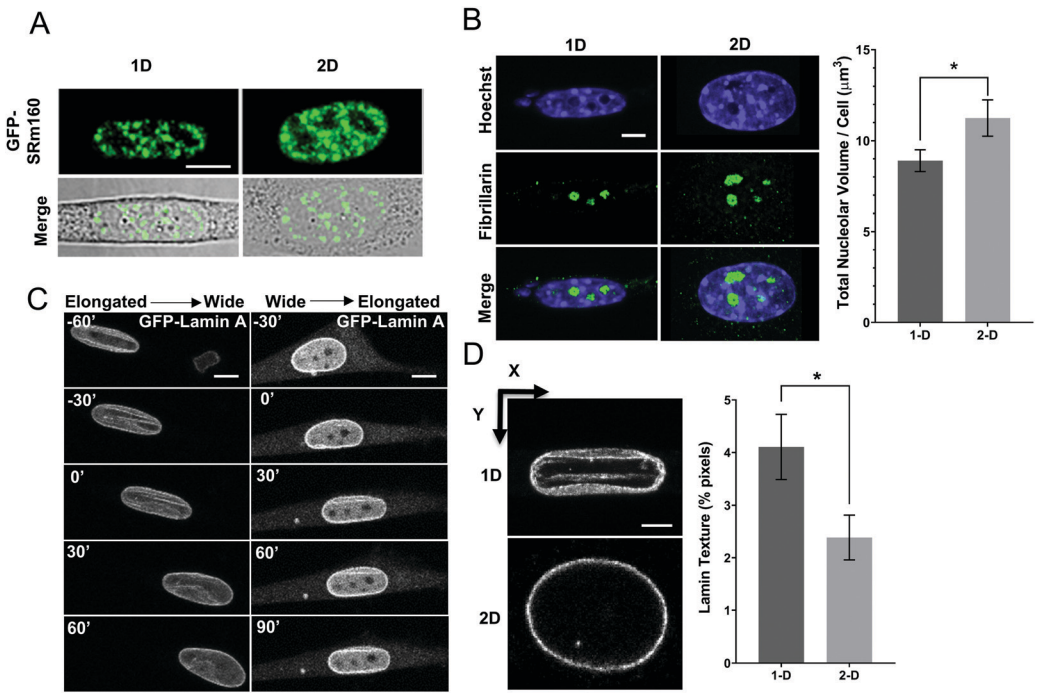

Fig. 3 Dilation of nuclear contents and unfolding of the nuclear lamina during the 1-D to 2-D transition. (A) Images of an NIH 3T3 fibroblast nucleus expressing splicing speckle protein GFP-SRm160 on the 1-D fibronectin line and subsequently on the 2-D region, along with overlays of the two images. Scale bar is 10 μm. (B) Images of fibroblast nuclei on 1-D fibronectin lines or 2-D fibronectin regions fixed and stained for fibrillarin, a nucleolar protein (green). Nuclei were counter-stained for DNA with Hoechst (blue). Scale bar is 5 μm. Plot compares total nucleolar volume per cell on 1-D lines (n = 43 cells from 3 independent experiments) and on 2-D fibronectin regions (n = 38 cells from 3 independent experiments). Data is mean ± SEM ($p < 0.05$ by Student's t-test). (C) Time lapse images of a NIH 3T3 fibroblast stably expressing GFP lamin a translating from a 1-D line to 2-D area (left column) and from a 2-D area to the 1-D line (right column). Scale bar is 10 μm. (D) Images of representative fibroblast nuclei on a 1-D line or 2-D area immunostained for lamin A/C. Scale bar is 5 μm. Plot shows lamin texture calculated as pixels in texture/total nuclear pixels × 100 in cells cultured on 1-D lines and 2-D areas. n = 34 cells on 1-D line and n = 36 cells on 2-D area; *$p < 0.05$ by Student's t-test. See Materials and methods for details of the texture calculation.

see Fig. S3, ESI,† and methods for more information). There was a statistically significant reduction in the texture on 2-D areas compared to 1-D lines (Fig. 3D). These results show that nuclear widening during migration is accompanied by dynamic unfolding of the nuclear lamina, consistent with similar observations during nuclear flattening[23] and during stretching of isolated nuclei.[24]

Nuclear volume correlates with cell volume

Changes in actomyosin tension alter nuclear volume.[14,15] For example, inhibiting myosin in fibroblasts spread on 2-D surfaces substantially reduced nuclear volume,[19] while inhibiting myosin in endothelial cells on 1-D lines increased nuclear volume.[25] Further, nuclear volume scales proportionately with cell volume.[8,9,13,26,27] Considering these previous studies, we reasoned that one potential mechanism for the observed differences in nuclear volume under different culture conditions and during cell widening during migration may be that the actomyosin-tension dependent cell volume is correspondingly altered under different culture conditions. However, reliable quantification of cell volume in cell shapes that vary widely in the different culture conditions proved to be difficult owing to the thin lamella and lamellipodia that are frequently below the *z*-resolution of the confocal microscope, and the branched three-dimensional morphologies in 3-D culture.

Motivated by the fact that volume measurements of rounded nuclei and rounded cells are far less limited by the difficulties of imaging lamellipodia, we devised an approach to quantify correlations between nuclear and cell volume, and the effects of inhibiting actomyosin tension on these properties. Spread cells were treated with three different types of pharmacological drugs, ML-7, a myosin light chain kinase inhibitor, blebbistatin, an inhibitor of non-muscle myosin II (NMMII) activity, and Y-27632, a Rho-kinase inhibitor for 60 minutes which allows efficient inhibition of NMMII in spread cells.[28] Any potential changes to cell volume and nuclear volume were likely to occur over this time period in NIH 3T3 fibroblasts.[15] Thereafter, cells were trypsinized and resuspended in fresh media in the presence of these inhibitors, and seeded on glass bottomed dishes. Next, these cells were fixed at around 10 minutes after cell seeding, which allowed sufficient time for cell adhesion but not

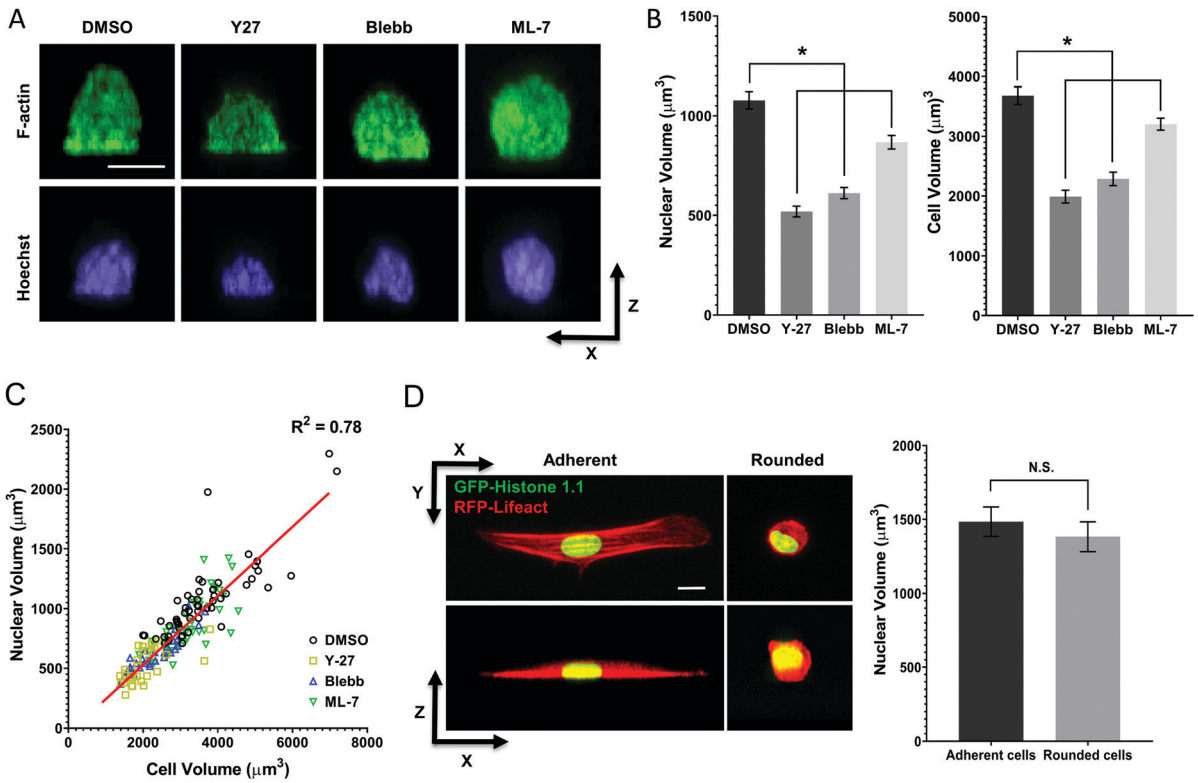

Fig. 4 Nuclear volume scales with cell volume. (A) Representative *x*–*z* images of the nucleus (blue, stained for DNA with Hoechst 33342) and the cell (green, stained for F-actin with alexa Fluor-488 phalloidin) treated with 25 μm ML-7, a myosin light chain kinase inhibitor, 50 μm Blebbistatin, an inhibitor of myosin activity, and 25 μm Y-27632, a Rho kinase inhibitor or DMSO control for 1 hour, before trypsinization and subsequent seeding on glass-bottomed dishes for 10 minutes, followed by fixation. Scale bar is 10 μm. (B) Quantification of cell and nuclear volume in the experiments corresponding to (A). Cell numbers quantified for DMSO, Y-27, Blebb and ML-7 were 55, 30, 30 and 45, respectively. Data is from three independent experiments. Data is mean ± SEM; $*p < 0.05$ by Student's *t*-test. (C) Scatter plot of nuclear volume *versus* cell volume from the data in (B). The red line was determined by linear regression; $R^2 = 0.78$. (D) Measurements of nuclear volume after cell rounding due to trypsinization. GFP-histone H1.1 tagged NIH 3T3 fibroblasts were detached from the dish by adding 0.083% trypsin. Cells were imaged with confocal microscopy until the cell became rounded. Representative images show the change of cell shape (red, RFP-lifeact) and nucleus (green, GFP-histone1.1) in *x*–*y* and *x*–*z* views before (adherent) and after trypsinization (rounded). Scale bar is 10 μm. Plot shows quantification of nuclear volume in adherent and rounded cells. All data are mean ± SEM from 14 different cells. n.s. signifies $p > 0.05$ by the Student's *t*-test.

spreading (Fig. 4A). Cells were round, and nuclei were correspondingly round at 10 minutes into the spreading process. There was a near absence of thin lamellar structures in these cells (Fig. 4A).

Treatment with each of these drugs significantly reduced nuclear volume, and also reduced cell volume (Fig. 4B). There was a clear correlation between cell and nuclear volume under these treatment conditions (Fig. 4C). Somewhat surprisingly, however, trypsinization of cells which has been suggested to cause a decrease in nuclear volume,[14] had no corresponding effect on nuclear volume (Fig. 4D and Movie 7, ESI†), which suggests that rapid relaxation of actomyosin tension is not sufficient to alter cell and nuclear volume. These results collectively suggest that nuclear volume changes caused by inhibition of actomyosin tension are correlated with cell volume changes.

Discussion

Elongated mammalian cells tend to contain elongated nuclei while circular cells contain rounder nuclei in different cell types.[25,29] Wide cell and nuclear shapes prevent extravasation through tight spaces in the extracellular matrix, while narrowing of the nucleus due to local cell constriction allows migratory escape.[30] The coordination between mammalian cell and nuclear shape is driven by motion of cellular boundaries toward and/or away from the nuclear surface.[15,29] There have been contrasting reports on the effect of cell shape and mechanics on nuclear volume. Nuclear volume was low in elongated micropatterned primary human umbilical vein endothelial cells,[25] while it was unchanged with elongation of human lung microvascular endothelial cells.[31] Nuclear volume was constant during the dynamic process of fibroblast spreading[15] and during the squeezing of wild type and lamin A/C deficient fibroblasts through narrow pores[32] but increased during spreading of microvascular endothelial cells.[31] Here, we show that a significant nuclear volumetric dilation is caused by local outward motion of cellular boundaries during fibroblast migration from 1-D to 2-D fibronectin patterns. This dilation is accompanied by the dilation of chromatin and other sub-nuclear structures like splicing speckles and nucleoli, and an unfolding of the nuclear lamina. Our observations are consistent with previous observations that nuclear volume scales inversely with the degree of elongation in micropatterned endothelial cells.[31]

We found that the volume of the nucleus is proportional to cell volume in cells allowed to adhere for very short times (Fig. 4). Furthermore, actomyosin inhibition reduced cell volume, and proportionately reduced nuclear volume. In these experiments, we trypsinized cells and allowed them to adhere but not spread on culture dishes. However, we found it difficult to measure changes in cell volume during migration or in different culture systems owing to errors introduced during the imaging of thin lamellipodia and/or irregular cell structures. Based on several recent studies in other systems which show that nuclear size is primarily determined by cytoplasmic volume,[8,10,11,13] and the fact that actomyosin tension is lower in elongated cells compared to more circular cells,[31] it is reasonable to speculate that the changes in nuclear volume during cell migration and in different culture conditions are a secondary effect of changes to cell volume caused by differences in actomyosin tension. Cell volume may not change during the process of spreading or migrating through tight spaces, which may explain why the nuclear volume is unchanged during these processes.[15,32] How cell volume might be altered differentially in these different situations is unclear at present, but is likely related to the overall actomyosin tension and the impact of actomyosin activity on mechanical properties[33] of the cell.

We also found systematic differences in nuclear volume in different modes of culture, which are consistent with the corresponding elongated *vs.* rounder nuclear phenotypes. Nuclear volume differences in these different culture conditions, and associated alterations to intranuclear structure[34] could potentially contribute to the systematic differences in gene expression and cell function between 2-D and 3-D culture.[35–39] Mechanical forces applied to the nuclear surface through magnetic manipulation of beads bound to the cell surface have been shown to stretch chromatin in the nucleus locally, and thereby alter gene expression.[40] Migration of cells through constricted spaces stretches chromatin,[41] causes nuclear rupture[42–45] and DNA damage.[46] Dynamic changes to nuclear size and associated intranuclear structure during cell motility may be an additional mechanism that impacts cell and nuclear functions.

Methods

Microcontact printing

Hydrophilic polymer tissue culture dishes (Ibidi, Martinsreid, Germany) were patterned by micro-contact printing as previously described.[47,48] Briefly, a silicon wafer was etched with the surface features using standard photolithography techniques. Then, Sylgard 184 (polydimethylsiloxane elastomer kit, Dow Corning, Midland, MI) was mixed in a 10 : 1 ratio and cured against the silicon wafer. Rhodamine-conjugated fibronectin (Cytoskeleton, Denver, CO), was diluted to 50 μg ml^{-1} and a 20 μl drop was adsorbed onto the stamp surface for 1 hour. Culture dishes were treated briefly with a handheld corona treatment unit (Model BD-20, Electro-Technic Products Inc., Chicago, IL) prior to contacting them with the rinsed and dried stamps. Non-printed regions of the dish were backfilled with 0.2 μg ml^{-1} PLL-*g*-PEG solution (Surface Solutions, Dübendorf, Switzerland) for 1 hour to prevent inadvertent protein adsorption. Substrates were stored up to 1 week at 4 °C in PBS.

Cell culture, transfection, and drug treatments

Cells were maintained in a humidified incubator at 37 °C and 7% CO_2. NIH 3T3 fibroblasts (ATCC CRL-1658) were cultured in Dulbecco's Modified Eagle's Medium (DMEM) with 4.5 g l^{-1} glucose (Mediatech, Manassas, VA), supplemented with 10% donor bovine serum (DBS, Gibco, Grand Island, NY) and 1% penicillin/streptomycin (Mediatech). For 3-D culture, cells were encapsulated in 3 mg ml^{-1} rat-tail collagen I gels (Ibidi) as

specified by the manufacturer protocols. Briefly, 5 mg ml^{-1} collagen was thawed, diluted and brought to physiological pH. Cells were suspended in the solution and transferred to a culture dish. Collagen fibers were allowed to polymerize at 37 °C for 30 minutes before normal cell culture. Transfections were performed with Lipofectamine 3000 (ThermoFisher Scientific, Waltham, MA) in OptiMEM serum-free media (ThermoFisher) following the manufacturers protocols. Dendra2-H3.3-N-14 was a gift from Michael Davidson (Addgene plasmid #57725) and GFP-SRm160 was a gift from Jeffrey Nickerson. NIH 3T3 fibroblasts stably expressing GFP-Lamin A were a kind gift from Kyle Roux. Myosin inhibition was accomplished by treating cells with 25 μM Y-27632 (EMD Millipore, Billerica, MA), 50 μM Blebbistatin (EMD Millipore Billerica, MA), or 25 μM ML-7 (Sigma-Aldrich, St. Louis, MO).

Immunostaining

For immunostaining experiments, cells were fixed in 4% paraformaldehyde at room temperature for 10 minutes, washed with PBS, and pre-treated with permeabilization buffer (PBS containing 0.1% Triton-X and 1% bovine serum albumin) for 15 minutes. The samples were incubated with mouse anti-fibrillarin (ab4566, Abcam) or mouse anti-lamin A (ab8980, Abcam); diluted in permeabilization buffer at 4 °C for 1 hour prior to secondary labeling with 488 goat-anti-mouse IgG antibody (ThermoFisher Scientific). The nucleus and F-actin were stained with Hoechst 33342 (Sigma-Aldrich, St. Louis, MO) and Alexa Fluor-488 phalloidin (ThermoFisher Scientific), respectively.

Fixed and live cell imaging

Imaging was performed on a Nikon A1+ laser scanning confocal microscope (Nikon, Melville, NY) with a 60×/1.4 NA oil immersion objective. For live cell imaging, cells were maintained at 37 °C and 5% CO_2 in a humidified chamber. A pinhole of 1 Airy disk with our 60×, 1.4 NA objective corresponds to a typical *z*-directional optical section of ~500 nm for a 488 nm laser beam. We chose our step size in the 300–400 nm step size, and performed imaging with a pinhole opening at about 1.5–1.8 Airy disks which ensured overlapping z-stacks while sampling below the Nyquist optical section (~400–500 nm) to minimize photobleaching artifacts. z-stacks for volume measurements were acquired with a 300 nm axial step size for fixed cell imaging, and 400 nm axial step size for live cell imaging; the higher axial step size for live cell imaging was done to minimize any photobleaching artifacts.

Photoconversion experiments were performed on Dendra2-histone H3.3 on a Nikon A1+ laser scanning confocal microscope. Cells were maintained at 37 °C and 5% CO_2 in a humidified chamber. The photoconversion was performed by irradiating a pre-defined spot with a 405 nm laser beam at 5–10% power, and images were collected in the green and red channels with 488 nm and 594 nm excitation lasers respectively.

In trypsinization experiments, GFP-histone and RFP-Lifeact labeled NIH3T3 cells were plated on fibronectin coated glass bottom dishes overnight. Before trypsinization, cells and nuclei were imaged with confocal microscope to construct z-stack for 30 minutes at 5 minute intervals. The cell media was then replaced with 0.083% trypsin. Changes in cell and nuclear cross-sections were recorded every 5 min using confocal z-stack imaging until cells completely detached from the dish.

Image analysis & measurement of nuclear properties

Fiji software[49] was used for all image processing and measurements. Image stacks (for 3-D measurements, such as volume) or maximum intensity projections (for 2-D measurements, such as cross-sectional area, length, and width) were segmented with an automatic threshold algorithm using the Yen thresholding criterion. Then, measurements were performed on included voxels/pixels using Fiji's built-in tools. Nucleoli were measured in the same fashion from fluorescent images of fibrillarin.

All lamin texture segmentation and analysis was quantified from immunolabeled lamin A images. First, the images were segmented using an Otsu segmentation algorithm. A pixel area size exclusion filter with empirically determined upper and lower limits was then applied to segmented objects to exclude small imaging artifacts. Second, the features within the nuclear lamina were detected through the application of a Laplacian of Gaussian filter. Third, the algorithm removed the contributions of the nuclear envelope from the quantification of 'texture' pixels within the lamina. The boundary of the nuclear envelope was detected using the Otsu method. A Sobel edge detection algorithm was then applied to the binary image to detect the nuclear periphery. This image was then subtracted from the texture-detected image generated in the second step of the algorithm to obtain a new image excluding any contributions from the nuclear periphery. Finally, the number of texture pixels were summed to yield a total number of texture pixels within each individual nucleus. A schematic of this method is provided in Fig. S3 (ESI†).

Conflicts of interest

There are no conflicts to declare.

Acknowledgements

This work was supported by the National Institutes of Health (grants R01 EB014869 to T.P.L.).

References

1 C. Denais and J. Lammerding, *Adv. Exp. Med. Biol.*, 2014, **773**, 435–470.
2 P. M. Davidson and J. Lammerding, *Trends Cell Biol.*, 2014, **24**, 247–256.
3 D. Zink, A. H. Fischer and J. A. Nickerson, *Nat. Rev. Cancer*, 2004, **4**, 677–687.
4 T. P. Lele, R. B. Dickinson and G. G. Gundersen, *J. Cell Biol.*, 2018, **217**, 3330–3342.
5 C. Uhler and G. V. Shivashankar, *Trends Cancer*, 2018, **4**, 320–331.

6 L. J. Edens, K. H. White, P. Jevtic, X. Li and D. L. Levy, *Trends Cell Biol.*, 2013, **23**, 151–159.
7 D. L. Levy and R. Heald, *Annu. Rev. Cell Dev. Biol.*, 2012, **28**, 113–135.
8 F. R. Neumann and P. Nurse, *J. Cell Biol.*, 2007, **179**, 593–600.
9 P. Jorgensen, N. P. Edgington, B. L. Schneider, I. Rupes, M. Tyers and B. Futcher, *Mol. Biol. Cell*, 2007, **18**, 3523–3532.
10 Y. Hara and C. A. Merten, *Dev. Cell*, 2015, **33**, 562–575.
11 D. L. Levy and R. Heald, *Cell*, 2010, **143**, 288–298.
12 M. Guo, A. F. Pegoraro, A. Mao, E. H. Zhou, P. R. Arany, Y. Han, D. T. Burnette, M. H. Jensen, K. E. Kasza, J. R. Moore, F. C. Mackintosh, J. J. Fredberg, D. J. Mooney, J. Lippincott-Schwartz and D. A. Weitz, *Proc. Natl. Acad. Sci. U. S. A.*, 2017, **114**, E8618–E8627.
13 J. D. Finan and F. Guilak, *J. Cell. Biochem.*, 2010, **109**, 460–467.
14 D. H. Kim, B. Li, F. Si, J. M. Phillip, D. Wirtz and S. X. Sun, *J. Cell Sci.*, 2016, **129**, 457.
15 Y. Li, D. Lovett, Q. Zhang, S. Neelam, R. A. Kuchibhotla, R. Zhu, G. G. Gundersen, T. P. Lele and R. B. Dickinson, *Biophys. J.*, 2015, **109**, 670–686.
16 J. R. Sims, S. Karp and D. E. Ingber, *J. Cell Sci.*, 1992, **103**(Pt 4), 1215–1222.
17 S. Munevar, Y. Wang and M. Dembo, *Biophys. J.*, 2001, **80**, 1744–1757.
18 S. Munevar, Y. L. Wang and M. Dembo, *Mol. Biol. Cell*, 2001, **12**, 3947–3954.
19 Y. Li, D. Lovett, Q. Zhang, S. Neelam, R. A. Kuchibhotla, R. Zhu, G. G. Gundersen, T. P. Lele and R. B. Dickinson, *Biophys. J.*, 2015, **109**, 670–686.
20 N. Naetar, S. Ferraioli and R. Foisner, *J. Cell Sci.*, 2017, **130**, 2087–2096.
21 H. Kimura and P. R. Cook, *J. Cell Biol.*, 2001, **153**, 1341–1353.
22 Q. Zhang, K. P. Kota, S. G. Alam, J. A. Nickerson, R. B. Dickinson and T. P. Lele, *J. Cell. Physiol.*, 2016, **231**, 1269–1275.
23 S. Neelam, P. R. Hayes, Q. Zhang, R. B. Dickinson and T. P. Lele, *Sci. Rep.*, 2016, **6**, 19689.
24 A. D. Stephens, E. J. Banigan, S. A. Adam, R. D. Goldman and J. F. Marko, *Mol. Biol. Cell*, 2017, **28**, 1984–1996.
25 M. Versaevel, T. Grevesse and S. Gabriele, *Nat. Commun.*, 2012, **3**, 671.
26 J. D. Finan, H. A. Leddy and F. Guilak, *Biochem. Biophys. Res. Commun.*, 2011, **408**, 230–235.
27 J. D. Finan, K. J. Chalut, A. Wax and F. Guilak, *Ann. Biomed. Eng.*, 2009, **37**, 477–491.
28 S. Kumar, I. Z. Maxwell, A. Heisterkamp, T. R. Polte, T. P. Lele, M. Salanga, E. Mazur and D. E. Ingber, *Biophys. J.*, 2006, **90**, 3762–3773.
29 V. J. Tocco, Y. Li, K. G. Christopher, J. H. Matthews, V. Aggarwal, L. Paschall, H. Luesch, J. D. Licht, R. B. Dickinson and T. P. Lele, *J. Cell. Physiol.*, 2018, **233**, 1446–1454.
30 K. Wolf, M. Te Lindert, M. Krause, S. Alexander, J. Te Riet, A. L. Willis, R. M. Hoffman, C. G. Figdor, S. J. Weiss and P. Friedl, *J. Cell Biol.*, 2013, **201**, 1069–1084.
31 P. Roca-Cusachs, J. Alcaraz, R. Sunyer, J. Samitier, R. Farré and D. Navajas, *Biophys. J.*, 2008, **94**, 4984–4995.
32 P. M. Davidson, J. Sliz, P. Isermann, C. Denais and J. Lammerding, *Integr. Biol.*, 2015, **7**, 1534–1546.
33 C. J. Chan, A. E. Ekpenyong, S. Golfier, W. Li, K. J. Chalut, O. Otto, J. Elgeti, J. Guck and F. Lautenschläger, *Biophys. J.*, 2015, **108**, 1856–1869.
34 C. Uhler and G. V. Shivashankar, *Nat. Rev. Mol. Cell Biol.*, 2017, **18**, 717–727.
35 R. Edmondson, J. J. Broglie, A. F. Adcock and L. Yang, *Assay Drug Dev. Technol.*, 2014, **12**, 207–218.
36 D. Antoni, H. Burckel, E. Josset and G. Noel, *Int. J. Mol. Sci.*, 2015, **16**, 5517–5527.
37 S. Sieh, A. V. Taubenberger, S. C. Rizzi, M. Sadowski, M. L. Lehman, A. Rockstroh, J. An, J. A. Clements, C. C. Nelson and D. W. Hutmacher, *PLoS One*, 2012, **7**, e40217.
38 A. C. Luca, S. Mersch, R. Deenen, S. Schmidt, I. Messner, K.-L. Schäfer, S. E. Baldus, W. Huckenbeck, R. P. Piekorz and W. T. Knoefel, *PLoS One*, 2013, **8**, e59689.
39 C. P. Gibbs, V. G. Kukekov, J. D. Reith, O. Tchigrinova, O. N. Suslov, E. W. Scott, S. C. Ghivizzani, T. N. Ignatova and D. A. Steindler, *Neoplasia*, 2005, **7**, 967–976.
40 A. Tajik, Y. Zhang, F. Wei, J. Sun, Q. Jia, W. Zhou, R. Singh, N. Khanna, A. S. Belmont and N. Wang, *Nat. Mater.*, 2016, **15**(12), 1287–1296.
41 J. Irianto, Y. Xia, C. R. Pfeifer, R. A. Greenberg and D. E. Discher, *Biophys. J.*, 2017, **112**, 446–449.
42 C. M. Denais, R. M. Gilbert, P. Isermann, A. L. McGregor, M. te Lindert, B. Weigelin, P. M. Davidson, P. Friedl, K. Wolf and J. Lammerding, *Science*, 2016, **352**, 353–358.
43 C. T. Halfmann, R. M. Sears, A. Katiyar, B. W. Busselman, L. K. Aman, Q. Zhang, C. S. O'Bryan, T. E. Angelini, T. P. Lele and K. J. Roux, *J. Cell Biol.*, 2019, **218**, 2136–2149.
44 E. M. Hatch and M. W. Hetzer, *J. Cell Biol.*, 2016, **215**, 27–36.
45 M. Raab, M. Gentili, H. de Belly, H. R. Thiam, P. Vargas, A. J. Jimenez, F. Lautenschlaeger, R. Voituriez, A. M. Lennon-Duménil, N. Manel and M. Piel, *Science*, 2016, **352**, 359–362.
46 C. R. Pfeifer, Y. Xia, K. Zhu, D. Liu, J. Irianto, V. M. M. Garcia, L. M. S. Millan, B. Niese, S. Harding, D. Deviri, R. A. Greenberg and D. E. Discher, *Mol. Biol. Cell*, 2018, **29**, 1948–1962.
47 G. Csucs, R. Michel, J. W. Lussi, M. Textor and G. Danuser, *Biomaterials*, 2003, **24**, 1713–1720.
48 M. Théry and M. Piel, *Cold Spring Harb. Protoc.*, 2009, **2009**, pdb.prot5255.
49 J. Schindelin, I. Arganda-Carreras, E. Frise, V. Kaynig, M. Longair, T. Pietzsch, S. Preibisch, C. Rueden, S. Saalfeld, B. Schmid, J. Y. Tinevez, D. J. White, V. Hartenstein, K. Eliceiri, P. Tomancak and A. Cardona, *Nat. Methods*, 2012, **9**, 676–682.

